Title

Progression of Self-Assembly of Amelogenin Protein Supramolecular Structures in Simulated Enamel Fluid

Journal

Biomacromolecules, 19(10)

ISSN

1525-7797

Authors

Engelberth, Sarah A
Bacino, Margot S
Sandhu, Shaiba
et al.

Publication Date

2018-10-08

DOI

10.1021/acs.biomac.8b00808

Peer reviewed

Published in final edited form as:

Biomacromolecules. 2018 October 08; 19(10): 3917–3924. doi:10.1021/acs.biomac.8b00808.

Progression of Self-Assembly of Amelogenin Protein Supramolecular Structures in Simulated Enamel Fluid

Sarah A. Engelberth[†], **Margot S. Barino**[†], **Shaiba Sandhu**[†], **Wu Li**[†], **Johan Bonde**[‡], **Stefan Habelitz**[*,†]

[†]Department of Preventive and Restorative Dental Sciences, University of California, San Francisco, 707 Parnassus Avenue, San Francisco, California 94143, United States

[‡]Division of Pure and Applied Biochemistry, Center for Applied Life Sciences, Lund University, P.O. Box 124, SE-221 00, Lund, Sweden

Abstract

Mechanisms of protein-guided mineralization in enamel, leading to organized fibrillar apatite nanocrystals, remain elusive. In vitro studies reveal recombinant human amelogenin (rH174), a matrix protein templating this process, self-assembles into a variety of structures. This study endeavors to clarify the self-assembly of rH174 in physiologically relevant conditions. Self-assembly in simulated enamel fluid was monitored up to 2 months. At alkali (7.3–8.7) and acidic (5.5–6.1) pH ranges, a distinct progression in formation was observed from nanospheres (17–23 nm) to intermediate-length nanorods, concluding with the formation of long 17–18 nm wide nanoribbons decorated with nanospheres. Assembly in acidic condition progressed quicker to nanoribbons with fewer persistent nanospheres. X-ray diffraction exhibited reflections characteristic of antiparallel β-sheets (4.7 and 9.65 Å), supporting the model of amyloid-like nanoribbon formation. This is the first observation of rH174 nanoribbons at alkaline pH as well as concurrent nanosphere formation, indicating both supramolecular structures are stable together under physiological conditions.

Graphical abstract

[*]**Corresponding Author** stefan.habelitz@ucsf.edu.

Author Contributions

The manuscript was written through contributions of all authors. All authors have given approval to the final version of the manuscript.

ASSOCIATED CONTENT

Supporting Information

The Supporting Information is available free of charge on the ACS Publications website at DOI: 10.1021/acs.bio-mac.8b00808.

pH study of carbonate buffering and XRD spectra and profiles of rH174 assembled in acidic and alkali conditions (PDF).

Notes

The authors declare no competing financial interest.

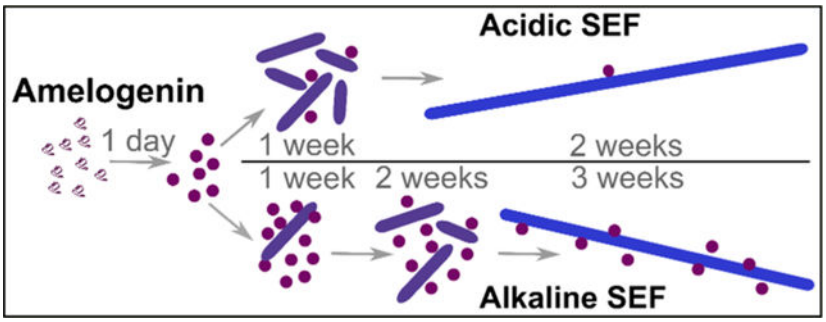

INTRODUCTION

Enamel is the hardest tissue in mammals and the outermost covering of the tooth. Mature enamel gets its strength from the microscopic arrangement of hydroxyapatite fibers, with an extremely high aspect ratio at 50 nm wide and up to hundreds of microns in length.[1] These crystalline fibers are further ordered into 4–5 μm diameter rods with interrrod micro-structure regions, providing resistance to chipping and crack propagation.[2] This structure is patterned during the secretory stage of amelogenesis, when an organic matrix is laid down by ameloblasts accompanied by initial formation of thin mineral ribbons of 2–4 nm thickness and 15–20 nm width.

During amelogenesis, ameloblast cells are responsible for excretion of the organic matrix template through the Tomes' process into the extracellular space. The resultant protein matrix is composed primarily of the protein amelogenin and its cleavage products (~90%), along with other proteins (ameloblastin, enamelin, amelotin, biglycan), which provide structural scaffolding for biological apatite ($Ca_5(PO_4, CO_3)_3(OH, F)$) crystal formation.[3–5] This scaffold is enzymatically processed initially by the enzyme matrix metalloproteinase-20 (MMP-20) and further degraded by kallikrein-related peptidase-4 (KLK-4) as the cells transition into the maturation phase, in which protein is removed from the extracellular space to allow for expansion of apatite mineral into fibers.

Due to this enzymatic cleavage of the organic matrix, only trace amounts of protein are detected in mature enamel. As such, the exact configuration of the protein structures in vivo during amelogenesis is difficult to verify. Several studies have shown the presence of cross-beta (cross-β) amyloid structures in developing enamel using X-ray Diffraction (XRD). The protein amelogenin is essential for proper enamel formation, as in the absence of amelogenin, a disorganized and prismless tissue that lacks the microstructural characteristic of mammalian enamel is formed.[6,7] Amelogenin is a hydrophobic protein with a hydrophilic C-terminal region. This C-terminus as well as the N-terminal region are highly conserved within mammalian species, accenting their importance during protein assembly and mineralization.[8] Amelogenin has demonstrated the ability to self-assemble into a variety of quaternary structures in vitro, most notably nanospheres and nanoribbons (Table 1), which may be responsible for the templating of enamel.

During the 1990s, investigation into the self-assembly of amelogenin indicated that the protein assembled into 12–18 nm nanospheres when incubated in 20 mM Tris-HCl (pH 8.0,

23 °C).[9] These nanospheres are proposed to assemble via intermediate 4–5 nm structures, composed of 4–6 nm amelogenin monomers assembled intracellularly prior to secretion into the matrix.[10,11] Nanosphere diameter is dependent on pH and temperature, sometimes aggregating into larger 60–70 nm particles at 37 °C.[12,13] When adsorbed onto charged surfaces and studied by Atomic Force Microscopy (AFM), nanospheres are destabilized and disaggregate, evidenced by small monomeric or oligomeric structures.[14–16] Based on observation of similar sphere-like structures in developing enamel using transmission electron microscopy (TEM), it was proposed that these nanospheres, assembled into bead-like chains, serve as the substrate for oriented hydroxyapatite mineral deposition.[17,18] However, the accurate interpretation of these TEM micrographs and the possibility of imaging artifacts has been called into question.[19]

More recently, filamentous or ribbon-like assemblies of amelogenin without nanosphere intermediates were observed in vitro by our laboratory.[24] Initial assemblies performed in an oil–water emulsion system containing calcium and phosphate, resulted in formation of 17 nm diameter nanoribbons that measured micrometers in length.[24,25] These structures are reproducible in an aqueous-only system resulting in similar ribbons. The formation of ribbons at acidic pH is likely driven by ion-bridged dimers assembling in parallel that then elongate into ribbons.[28] The inclusion of both calcium and phosphate, the major mineral components of hydroxyapatite, are necessary for direct ribbon formation.[28] XRD of these ribbons exhibits a 4.7 Å peak, indicative of β-sheet conformation that correlates well to diffraction patterns of developing bovine enamel.[29] This spacing is also consistent with cross-β configuration of structural amyloids, which have been detected in developing murine enamel.[27] Further in silico studies have highlighted several different peptide domains within amelogenin that have a high likelihood to form β-sheets.[26]

Both the nanosphere and nanoribbon models are assembled in conditions that are not physiological in respect to pH or ionic composition (Table 1). The alkaline pH 8.0 that drives nanosphere formation and the acidic pH 5.5 resulting in nanoribbons lie at the extrema of what is found during amelogenesis. DLS studies have confirmed that amelogenin assembly is tightly regulated by pH.[30] A study of developing bovine enamel indicates that enamel tissue is composed of alternating acidic (pH 5.8–6.0) and neutral (pH 7.0–7.2) regions, attributed to pH neutralization mechanisms by ameloblasts.[31] Similar fluctuations occur in rat incisor enamel between acidic (pH 6.2–6.8) and neutral regions (pH 7.2) during maturation. This variation in pH may also be attributed to the process of mineralization.[32,33] The mineral composition of both the nanosphere and nanoribbon systems also do not reflect that of physiological enamel fluid, especially in respect to calcium and phosphate, the ionic components of hydroxyapatite. Nanoribbons are formed at high ionic concentrations of calcium and phosphate (3–33 and 2–21 mM, respectively). Conversely nanosphere formation has been reported in the absence of both mineral ions and nanospheres are destabilized when exposed to calcium and phosphate ions.[28]

As mature enamel lacks a cellular component, it is unable to regenerate. Thus, the understanding of amelogenin self-assembly at physiological conditions, the study of biomineralization during amelogenesis, and engineering of enamel mimetics as a restorative material, are of high priority.[34] In this study, in order to explore how amelogenin self-

assembly may occur in vivo, we sought to more closely mimic physiological conditions. As such, we utilized simulated enamel fluid (SEF), a solution based on the ionic components of immature secretory porcine enamel defined by Aoba et al. (Table 1).[20] Herein, we investigate the self-assembly of recombinant human amelogenin (rH174) in SEF at two different pH ranges at 37 °C, utilizing AFM, TEM, and XRD analysis.

EXPERIMENTAL SECTION

Materials.

Recombinant human amelogenin (rH174) was synthesized by expression in BL21DE3 pLyS *Escherichia coli,* as previously described.[26,35] Sodium fluoride was from Santa Cruz Biotechnology (Dallas, TX). Dipotassium phosphate was from Mallinckrodt Pharmaceuticals (St. Louis, MO). Sodium azide, magnesium chloride, and potassium chloride were from Thermo Fisher Scientific (Waltham, MA). All other reagents were purchased from Sigma-Aldrich (St. Louis, MO). Statistical analyses were performed using Origin Pro 8.5.1.

Protein Self-Assembly.

rH174 was dissolved at 2 mg/mL in 1 mM HCl and allowed to incubate overnight at 4 °C to ensure dissolution. Assembly was initiated by mixing 2× SEF at a 1:1 ratio with protein solution, yielding final concentrations described by Aoba et al. (0.15 mM $CaCl_2$, 3.9 mM K_2HPO_4, 0.83 mM $MgCl_2$, 13.2 mM KCl, 129 mM NaCl, 10 mM $NaHCO_3$, and 0.005 mM NaF).[20] Sodium azide was added as an antibacterial to a final concentration of 0.03 wt %. Reaction solutions were then pH adjusted to either 5.5 or 7.3 using 0.1 M HCl or 0.1 M KOH, respectively. Samples were incubated at 37 °C, without addition of an organic buffer. The pH was measured at relevant time points and recorded using a micro-pH combination glass-electrode (Sigma-Aldrich). Self-assembly was monitored in three independent replicate experiments.

Atomic Force Microscopy (AFM).

Samples were prepared for AFM at various time points. pH of assembly solution was recorded and then 15 μL of solution deposited on freshly cleaved muscovite mica (Electron Microscopy Science, Hatfield, PA) or glass coverslip (Fisher Scientific). The substrate was incubated with the sample in a wet cell at 37 °C for 30 min. Remaining moisture was wicked away using a Kimwipe (Kimtech Science) and rinsed with 30 μL of distilled water, followed by wicking and air drying. AFM was performed on a Bruker Multimode 8 with Nanoscope V controller (Bruker, Santa Barbara, CA) in air using silicon cantilevers (Bruker ScanAsyst Air-HR or Peakforce-HIRS-F-A) in Quantitative Nanomechanical Mapping Mode. Micrographs were flattened and dimensions analyzed using Nanoscope Analysis v1.8 and ImageJ.

Transmission Electron Microscopy (TEM).

TEM samples were prepared on Formvar coated 200 mesh copper grids (Ted Pella Inc., Redding, CA). A total of 10 μL of assembly solution was incubated for 2 min on the grid. Solution was wicked away and the grid incubated on a droplet of 2% methylamine tungstate

(Nano-W, Nanoprobes Yaphank, NY) for 10 s, prior to liquid removal and rinsing for 5 s on a droplet of 0.02 μm filtered distilled water. Ambient temperature TEM was performed using a Tecnai T12 TEM (FEI Company, Hillsboro, OR) or JEOL JEM1400 (JEOL USA Inc., Pleasanton, CA) operating at 120 keV. Data was recorded with a 4 × 4 Gatan Ultra Scan CCD camera (Gatan, Pleasanton, CA).

X-ray Diffraction (XRD).

Powder XRD was performed at beamline 8.3.1 at the Advanced Light Source at Lawrence Berkeley National Laboratory using 0.11159 nm synchrotron radiation. Nanoribbon samples were synthesized as described above with the following change. One week prior to XRD collection, following 7 weeks of nanoribbon assembly, solutions were concentrated to approximately 2 mg/mL protein and 2× SEF by dehydration in order to encourage sample aggregation. This process was performed to eliminate the addition of precipitants for crystallization. Aggregates were directly scooped from 30 μL of solution using MicroMeshes with a 400 μm aperture and 10 μm mesh holes (MiTeGen, Ithaca, NY). Partially hydrated samples were measured immediately. Diffraction patterns for rH174 assembled at both acidic and alkaline conditions, and a control of SEF salt alone was analyzed. XRD images were analyzed using FIT2D.[36] Images were background subtracted for a blank sample grid collected at the conclusion of the session under the same scan parameters (4 s scan of 100 μm spot size with 180° sample tilt at 250 mm distance to detector), followed by Q-space radial integration. Profiles were analyzed using Origin Pro 8.5.1 and peaks assigned manually.

RESULTS AND DISCUSSION

pH Assembly of rH174.

Protein was incubated in SEF at the initial pH of 5.5 and 7.3 at 37 °C. However, an increase in pH was observed over time in both solution conditions, rising to 6.1 and 8.7, respectively (Figure 1). This repeatable phenomenon was independent of the inclusion of protein ($p < 0.05$), occurring in control samples of solvent alone. This rise in pH occurred in as little as 6 h and has been attributed to the release of carbonate from SEF solution over time. A similar increase was observed in the literature in biological cell culture systems containing at least 1.8 mM carbonate.[37,38] When SEF of either pH was incubated in a cell culture 5% CO_2 incubator at 37 °C, this increase in pH was mitigated and pH held constant over incubation for up to 7 days, attributed to carbonate buffering (Figure S1). As such, the self-assembly reactions occurred at either the acidic range of 5.5–6.1 or an alkali range of 7.3–8.7. The acidic range tested is more physiological, spanning the range of pHs reported in developing enamel (5.8–6.0 and 7.0–7.2).[31,32] The increasing pH at the alkali range, while originally intended to correspond to physiological pH of 7.3, reaches values above the pH of developing enamel within 1 week.

Progression of Nanostructure Formation (AFM).

AFM analysis showed a common progression of nanostructure formation when comparing the two pH ranges, with varying speeds of morphology change. In the alkaline sample, after 1 week incubation nanospheres (Figure 2A, 22.9 ± 3.0 nm diameter) appeared. (Herein, we

will refer to 17–23 nm spherical superstructures as nanospheres. These are similar in size to the ~26 nm hydrodynamic diameter amelogenin spheres measured by DLS16 and recently reported 20–25 nm amelogenin subunits measured by TEM. 9) At 2 weeks, nanorods were observed (defined by an aspect ratio of 1.5–10) in addition to spheres (Figure 2B). Beginning at 3 weeks, nanoribbons (aspect ratio greater than 10) were observed, initially decorated with nanospheres. A dense network was formed by 4 weeks with a reduction in the number of nanospheres (Figure 2C). This is the first observation of nanoribbon formation at alkaline pH range in aqueous systems. However, at alkaline pH in SEF, nanoribbons required an incubation of almost three times longer than that observed previously at pH 4.5–5.5 with high concentrations of calcium and phosphate.28 Nanoribbon formation at the acidic pH range occurred quicker, with nanoribbons forming within 2 weeks (Figure 3C). Nanospheres (19.0 ± 2.7 nm diameter), first observed at 1 day of incubation (Figure 3A), progressed to a nanorod population (16.6 ± 1.3 nm width) within 1 week (Figure 3B). The resultant nanoribbons at 2 weeks (Figure 3C, 18.1 ± 3.6 nm width) were similar in morphology to those previously synthesized at acidic pH.[28]

A population analysis of the superstructures over time (Figure 4A,B) demonstrates the differing evolution of morphologies as a function of pH. Initially, at 1 day, the population distributions are the same at either pH, dominated by 98% nanospheres with few rods. However, by 1 week, the populations were markedly different, with no change in the alkaline assemblies and a nanorod-dominated population for assemblies incubated in the acidic range. This quick dissolution of nanospheres at acidic pH has been previously observed and has been attributed to the protonation of histidines (pK_a 6.0–6.5) within rH174.[28] At pH below 6, the positive charge of 14 histidines within the protein causes repulsion within monomers and limits hydrophobic interactions that may be essential for nanosphere formation.[39] We attribute the increased stability of nanospheres at alkaline pH to the deprotonation of the histidines and stabilization of nanosphere aggregates by hydrophobic interactions. In vivo, sphere destabilization may also be impacted by enzymatic degradation by MMP20 and KLK-4.

The diameter of the nanospheres at both conditions does not change significantly over the course of incubation (Figure 4C). While all spheres are in the same range of diameters (17–23 nm), there was a statistically significant difference in the diameter of the assemblies as a function of assembly pH. This is an indication of difference in tertiary structure of nanospheres formed at the acidic and alkaline assembly conditions. Both structures are likely formed from smaller oligomers via hydrophobic interactions, as previously reported at alkaline conditions,[16,39,40] but with differing folding behavior due to sensitivity to pH change. However, there was no discernible trend of nanosphere size being larger at one particular assembly pH, as nanospheres assembled in the acidic conditions were larger than alkaline-assembled nanospheres at 1 week, but slightly smaller at 2 weeks (Figure 4C).

Comparison of Nanosphere Stability (TEM).

When imaged with negatively stained (methylamine tungstate) TEM, nanospheres were clearly distinguished from nanoribbons (Figure 5A). In alkaline pH, both superstructures remained stable together in solution up to 8 weeks (Figure 5B) with no statistically

significant change in either 16.4 ± 3.3 nm nanoribbon or 20.2 ± 2.4 nm nanosphere diameter (Figure 6). While sphere formation commonly occurs at pH 8.0, to our knowledge, this was the first observation of long-term concurrent stability of nanoribbons and nanospheres. At the acidic pH range, occasional nanospheres were also detected by TEM at 3 weeks (Figure 5B) and 8 weeks (Figure 5D). The width of acidic-assembled nanoribbons increased from 10.4 ± 1.7 nm at 3 weeks to 17.6 ± 4.8 nm at 8 weeks. The spheres observed in acidic conditions were present at such a low density that statistical analysis of sphere dimensions could not be performed (Figure 5D). The formation of different morphologies at acidic and alkali pH, as well as the concurrent appearance of nanospheres and nanoribbons, opens future discussion for a functional role of multiple superstructures throughout enamel formation.

The distinct progression from nanosphere to nanorod to nanoribbon was conserved, regardless of the pH of the physiological ionic environment. The formation of larger structures from nanospheres may occur by two possible mechanisms: (A) spheres may align, as in the aligned nanosphere chains observed in TEM of developing enamel[1,17] and subsequently fuse into larger structures or (B) nanosphere disassembly into lower order structures (monomers, dimers, or oligomers) is followed by subsequent amelogenin self-assembly into larger, more stable structures. In both pH ranges of SEF assembly, nanospheres were observed in large groups, reminiscent of bunches of grapes, or later, aligned along the nanoribbons. However, at no time point was there evidence of the fusion of two or more nanospheres into a larger structure using either AFM or TEM analyses. There were also no trends in nanorod length to indicate they were formed by discrete numbers of nanospheres following fusion. Therefore, it is more probable that some degree of sphere disassembly drives the formation of larger superstructures.

Structural Analysis (XRD).

XRD of rH174 self-assemblies was performed using synchrotron radiation at the Alternative Light Source (Figure S3). Nanoribbons in acidic pH had an amyloid-like tertiary structure, exhibiting a reflection at 4.67 Å and a broader diffraction signal around 9.65 Å (Figure 7). The latter spacing is associated with antiparallel cross-β stacking between β-sheets, characteristic of amyloids. This is the first time that this spacing was detected in nanoribbon assemblies of amelogenin in vitro and is consistent with our model of nanoribbon formation, in which hydrogen bonding drives the formation of β-sheets from dimers followed by β-sheet stacking due to calcium bridges between glutamate and phosphoserine residues.[26] Other moderately strong reflections were observed at 3.64 and 6.88 Å, which correspond well with reflections observed in traditional amyloids.[41]

Despite having very similar morphologies, self-assemblies conducted at alkaline and acidic pH ranges had markedly different XRD profiles (Figures 7, S3, and S4). The alkaline-assembled nanoribbons had spacings at 5.2 Å, possibly corresponding to β-sheet structures. However, only a minor peak was detected at 9.35 E, which cannot corroborate cross β-sheet stacking. An unknown broad peak at 6.0 Å was also detected, which may be attributed to spacing within nano-spheres or other superstructures. However, in-depth studies on isolated

populations would be necessary prior to correlating this peak with any specific structural spacings.

CONCLUSIONS

In this study, rH174 self-assembled into nanoribbons when incubated at 37 °C in SEF, with the appearance of concurrent nanospheres at alkali pH. These superstructures have only been reported together in the literature for short incubations, yet were observed simultaneously in SEF for up to 8 weeks. In acidic conditions, nanospheres quickly transition into nanorods at 1 week and nanoribbons by 2 weeks. In contrast, at alkaline conditions, nanospheres were present at a higher density at all time points and transitioned more slowly to larger structures, requiring 3 weeks before the formation of nanoribbons. The same calcium-dependent mechanism is likely responsible for the formation of nanoribbons,[26] but the progression occurs at different speeds due to the increased stability of nanospheres at the alkaline condition. XRD of nanostructures formed at acidic and alkali conditions exhibit spacings consistent with β-sheets in similar conformations, 4.7 and 5.2 Å, respectively. This is indicative of amyloids and in agreement with previously reported spacing in amelogenin nanoribbons.[27] Nanoribbons assembled in acidic conditions have higher agreement with the XRD profiles of traditional amyloids, revealing antiparallel β-sheet spacing (9.6 Å reflection), and further supporting the in silico model of amyloid-like nanoribbon formation at acidic pH.[26]

As this study most closely mimics the conditions for protein self-assembly in vivo to date, it highlights the difficulty of mimicking the in vivo environment during amelogenesis. While, currently, SEF most closely mimics the physiological environment, it contains a very low calcium concentration. This is likely due to bound calcium or precipitated calcium salts that were not detected in the analysis of extracted enamel fluid.[42] As such, the actual concentration of this key ion during amelogenesis remains uncertain. Also, as previously discussed, due to a lack of carbonate buffering in atmospheric conditions, pH increased during incubation, and only the acidic condition remained in a physiologically relevant range. Finally, our use of rH174 also deviates from physiological conditions. rH174 lacks phosphorylation, whereas in human amelogenin, serine-16 is phosphorylated, which has been postulated to play a large role in assembly.[43] Future studies must be designed to overcome these hurdles, as well as incorporate other matrix proteins, in order to more closely mirror the physiochemical conditions of amelogenesis. Despite these limitations, this study highlights the importance of taking physiological conditions into account, as self-assembly of tertiary and quaternary structures is highly sensitive to environmental conditions. The structures formed at both pH ranges reveal the propensity of amelogenin to self-assemble into nanoribbons over time, which we postulate may be further enhanced at increased calcium concentration or higher protein concentrations associated with amelogenesis. The concurrent stability of nanosphere and nanoribbon superstructures calls into question if the hierarchical self-assembly of rH174 also results in a hierarchy of superstructures in vivo, which may together template hydroxyapatite growth.

Supplementary Material

Refer to Web version on PubMed Central for supplementary material.

ACKNOWLEDGMENTS

A portion of this work was conducted at the Advanced Light Source national user facility operated by the University of California (Office of the President, Multicampus Research Programs and Initiatives Grant MR-15–328599), the National Institutes of Health (R01 GM124149 and P30 GM124169), Plexxikon Inc., and the U.S. Department of Energy under Contract Number DE-AC02–05CH11231.

Funding

Funding to S.H., NIH/NIDCR R01-DE25709, and to J.B. from STINT, The Swedish Foundation for International Cooperation in Research and Higher Education.

REFERENCES

(1). Warshawsky H Organization of crystals in enamel. Anat. Rec. 1989, 224 (2), 242–62. [PubMed: 2672889]

(2). Habelitz S Materials engineering by ameloblasts. J. Dent. Res. 2015, 94 (6), 759–67. [PubMed: 25800708]

(3). Bartlett JD; Ganss B; Goldberg M; Moradian-Oldak J; Paine ML; Snead ML; Wen X; White SN; Zhou YL Protein–Protein Interactions of the Developing Enamel Matrix. Curr. Top. Dev. Biol. 2006, 74, 57–115. [PubMed: 16860665]

(4). Diekwisch T; David S; Bringas P; Santos V; Slavkin HC Antisense inhibition of AMEL translation demonstrates supra-molecular controls for enamel HAP crystal growth during embryonic mouse molar development. Development 1993, 117 (2), 471–482. [PubMed: 8392462]

(5). Diekwisch TG; Berman BJ; Gentner S; Slavkin HC Initial enamel crystals are not spatially associated with mineralized dentine. Cell Tissue Res. 1995, 279 (1), 149–167. [PubMed: 7895256]

(6). Bartlett JD Dental enamel development: proteinases and their enamel matrix substrates. ISRN Dent 2013, 2013, 684607.

(7). Gibson CW; Yuan Z-A; Hall B; Longenecker G; Chen E; Thyagarajan T; Sreenath T; Wright JT; Decker S; Piddington R Amelogenin-deficient mice display an amelogenesis imperfecta phenotype. J. Biol. Chem. 2001, 276 (34), 31871–31875. [PubMed: 11406633]

(8). Ruan Q; Moradian-Oldak J Amelogenin and Enamel Biomimetics. J. Mater. Chem. B 2015, 3, 3112–3129. [PubMed: 26251723]

(9). Fincham AG; Moradian-Oldak J; Simmer JP; Sarte P; Lau EC; Diekwisch T; Slavkin HC Self-assembly of a recombinant amelogenin protein generates supramolecular structures. J. Struct. Biol. 1994, 112 (2), 103–9. [PubMed: 8060728]

(10). Brookes SJ; Lyngstadaas SP; Robinson C; Shore RC; Kirkham J Intracellular nanosphere subunit assembly as revealed by amelogenin molecular cross-linking studies. Eur. J. Oral Sci. 2006, 114 (Suppl 1), 280–284. [PubMed: 16674699]

(11). Fincham AG; Leung W; Tan J; Moradian-Oldak J Does amelogenin nanosphere assembly proceed through intermediary-sized structures? Connect. Connect. Tissue Res. 1998, 38 (1–4), 237–40. [PubMed: 11063031]

(12). Wen HB; Fincham AG; Moradian-Oldak J Progressive accretion of amelogenin molecules during nanospheres assembly revealed by atomic force microscopy. Matrix Biol. 2001, 20 (5–6), 387–95. [PubMed: 11566273]

(13). Moradian-Oldak J; Leung W; Fincham AG Temperature and pH-dependent supramolecular self-assembly of amelogenin molecules: a dynamic light-scattering analysis. J. Struct. Biol. 1998, 122 (3), 320–7. [PubMed: 9774536]

(14). Tarasevich BJ; Lea S; Bernt W; Engelhard MH; Shaw WJ Changes in the quaternary structure of amelogenin when adsorbed onto surfaces. Biopolymers 2009, 91 (2), 103–7. [PubMed: 19025992]

(15). Tarasevich BJ; Lea S; Bernt W; Engelhard M; Shaw WJ Adsorption of amelogenin onto self-assembled and fluoroapatite surfaces. J. Phys. Chem. B 2009, 113 (7), 1833–42. [PubMed: 19199690]

(16). Chen CL; Bromley KM; Moradian-Oldak J; DeYoreo JJ In situ AFM study of amelogenin assembly and disassembly dynamics on charged surfaces provides insights on matrix protein self-assembly. J. Am. Chem. Soc. 2011, 133 (43), 17406–13. [PubMed: 21916473]

(17). Fincham AG; Moradian-Oldak J; Diekwisch TG; Lyaruu DM; Wright JT; Bringas P Jr.; Slavkin HC Evidence for amelogenin “nanospheres” as functional components of secretory-stage enamel matrix. J. Struct. Biol. 1995, 115 (1), 50–9. [PubMed: 7577231]

(18). Du C; Falini G; Fermani S; Abbott C; Moradian-Oldak J Supramolecular assembly of amelogenin nanospheres into birefringent microribbons. Science 2005, 307 (5714), 1450–1454. [PubMed: 15746422]

(19). Pandya M; Lin T; Li L; Allen MJ; Jin T; Luan X; Diekwisch TGH Posttranslational Amelogenin Processing and Changes in Matrix Assembly during Enamel Development. Front. Physiol. 2017, 8, 790. [PubMed: 29089900]

(20). Aoba T; Moreno EC The enamel fluid in the early secretory stage of porcine amelogenesis: chemical composition and saturation with respect to enamel mineral. Calcif. Tissue Int. 1987, 41 (2), 86–94. [PubMed: 3115550]

(21). Fang PA; Conway JF; Margolis HC; Simmer JP; Beniash E Hierarchical self-assembly of amelogenin and the regulation of biomineralization at the nanoscale. Proc. Natl. Acad. Sci. U. S. A. 2011, 108 (34), 14097–102. [PubMed: 21825148]

(22). Bonde J; Bulow L Random mutagenesis of amelogenin for engineering protein nanoparticles. Biotechnol. Bioeng. 2015, 112 (7), 1319–26. [PubMed: 25664685]

(23). Moradian-Oldak J; Du C; Falini G On the formation of amelogenin microribbons. Eur. J. Oral Sci. 2006, 114 (Suppl 1), 289–96. [PubMed: 16674701]

(24). He X; Wu S; Martinez-Avila O; Cheng Y; Habelitz S Self-aligning amelogenin nanoribbons in oil-water system. J. Struct. Biol. 2011, 174 (1), 203–12. [PubMed: 21134461]

(25). Martinez-Avila OM; Wu S; Cheng Y; Lee R; Khan F; Habelitz S Self-assembly of amelogenin proteins at the water-oil interface. Eur. J. Oral Sci. 2011, 119, 75–82. [PubMed: 22243231]

(26). Carneiro KMM; Zhai H; Zhu L; Horst JA; Sitlin M; Nguyen M; Wagner M; Simpliciano C; Milder M; Chen C-L; Ashby P; Bonde J; Li W; Habelitz S Amyloid-like ribbons of amelogenins in enamel mineralization. Sci. Rep. 2016, 6, 23105.

(27). Sanii B; Martinez-Avila O; Simpliciano C; Zuckermann RN; Habelitz S Matching 4.7-A XRD spacing in amelogenin nanoribbons and enamel matrix. J. Dent. Res. 2014, 93 (9), 918–22. [PubMed: 25048248]

(28). Martinez-Avila O; Wu S; Kim SJ; Cheng Y; Khan F; Samudrala R; Sali A; Horst JA; Habelitz S Self-assembly of filamentous amelogenin requires calcium and phosphate: from dimers via nanoribbons to fibrils. Biomacromolecules 2012, 13 (11), 3494–502. [PubMed: 22974364]

(29). Glimcher MJ; Daniel EJ; Travis DF; Kamhi S Electron optical and X-ray diffraction studies of the organization of the inorganic crystals in embryonic bovine enamel. J. Ultrastruct. Res. 1965, 12, 1–77. [PubMed: 14289428]

(30). Wiedemann-Bidlack FB; Beniash E; Yamakoshi Y; Simmer JP; Margolis HC pH triggered self-assembly of native and recombinant amelogenins under physiological pH and temperature in vitro. J. Struct. Biol. 2007, 160 (1), 57–69. [PubMed: 17719243]

(31). Sasaki S; Takagi T; Suzuki M Cyclical changes in pH in bovine developing enamel as sequential bands. Arch. Oral Biol. 1991, 36 (3), 227–231. [PubMed: 1877895]

(32). Smith CE; Issid M; Margolis HC; Moreno E Developmental changes in the pH of enamel fluid and its effects on matrix-resident proteinases. Advanced Dental Research 1996, 10 (2), 159–169.

(33). Lyman GE; Waddell WJ pH gradients in the developing teeth of young mice from autoradiography of [14C] DMO. American Journal of Physiology-Renal Physiology 1977, 232 (4), F364–F367.

(34). Klein OD; Duverger O; Shaw W; Lacruz RS; Joester D; Moradian-Oldak J; Pugach MK; Wright JT; Millar SE; Kulkarni AB; Bartlett JD; Diekwisch TG; DenBesten P; Simmer JP Meeting report: a hard look at the state of enamel research. Int. J. Oral Sci 2017, 9 (11), e3. [PubMed: 29165423]

(35). Bonde JS; Bulow L One-step purification of recombinant human amelogenin and use of amelogenin as a fusion partner. PLoS One 2012, 7 (3), e33269.

(36). Hammersley A FIT2D: An Introduction and Overview. ESRF Internal Report, 1997.

(37). Vistica DT; Scudiero D; Skehan P; Monks A; Boyd MR New carbon dioxide-independent basal growth medium for culture of diverse tumor and nontumor cells of human and nonhuman origin. J. Natl. Cancerlnst. 1990, 82 (12), 1055–61.

(38). Lelong IH; Rebel G pH drift of “physiological buffers” and culture media used for cell incubation during in vitro studies. J. Pharmacol. Toxicol. Methods 1998, 39 (4), 203–10. [PubMed: 9845299]

(39). Bromley KM; Kiss AS; Lokappa SB; Lakshminarayanan R; Fan D; Ndao M; Evans JS; Moradian-Oldak J Dissecting amelogenin protein nanospheres: characterization of metastable oligomers. J. Biol. Chem. 2011, 286 (40), 34643–53. [PubMed: 21840988]

(40). Ndao M; Dutta K; Bromley KM; Lakshminarayanan R; Sun Z; Rewari G; Moradian-Oldak J; Evans JS Probing the self-association, intermolecular contacts, and folding propensity of amelogenin. Protein Sci. 2011, 20 (4), 724–34. [PubMed: 21351181]

(41). Inouye H; Fraser P; Kirschner D Structure of B-crystallite assemblies formed by Alzheimer B-amyloid protein analogues: analysis by x-ray diffraction. Biophys. J. 1993, 64, 502–519. [PubMed: 8457674]

(42). Aoba T; Tanabe T; Moreno E Proteins in the enamel fluid of immature porcine teeth. J. Dent. Res. 1987, 66 (12), 1721–1726. [PubMed: 3479471]

(43). Wiedemann-Bidlack FB; Kwak S-Y; Beniash E; Yamakoshi Y; Simmer JP; Margolis HC Effects of phosphorylation on the self-assembly of native full-length porcine amelogenin and its regulation of calcium phosphate formation in vitro. J. Struct. Biol. 2011, 173 (2), 250–260. [PubMed: 21074619]

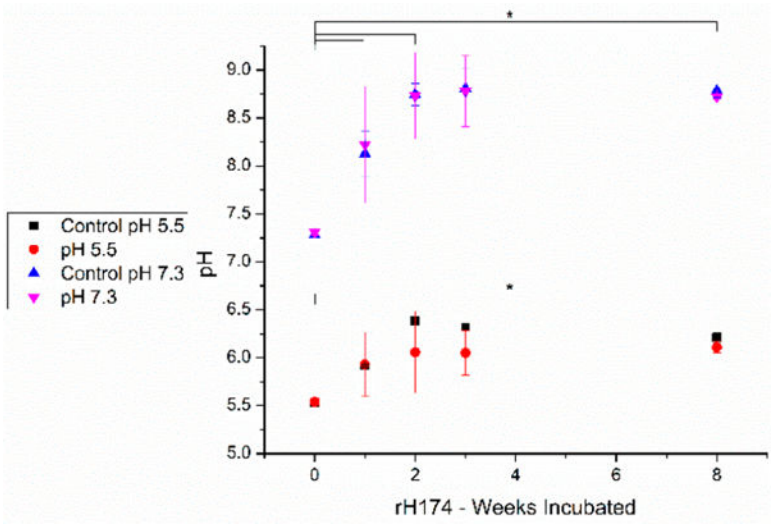

Figure 1.

pH increases during incubation of SEF solutions at 37 °C with and without rH174 protein (control) over 8 weeks. There is no statistical difference of pH value changes between control and protein samples at acidic or alkaline pH ranges (mean ± standard deviation, n = 3 independent experiments, $*p < 0.05$ determined by one-way ANOVA with Tukey's posthoc test).

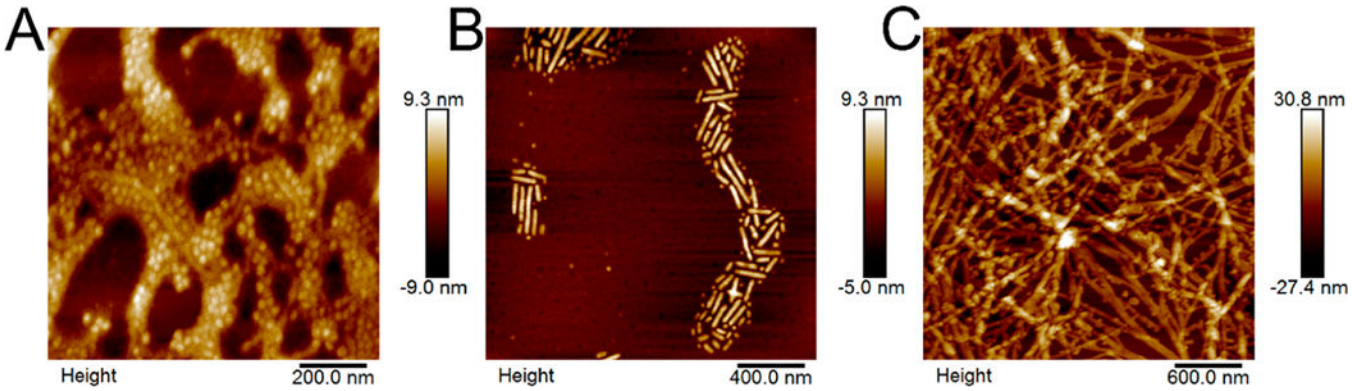

Figure 2.

rH174 nanostructures formed in SEF at alkaline pH progress from nanospheres at 1 week (A) to nanorods with nanospheres at 2 weeks (B) to nanoribbons over the course of 4 weeks (C) at 37 °C. Representative AFM micrographs of $n = 3$ independent syntheses.

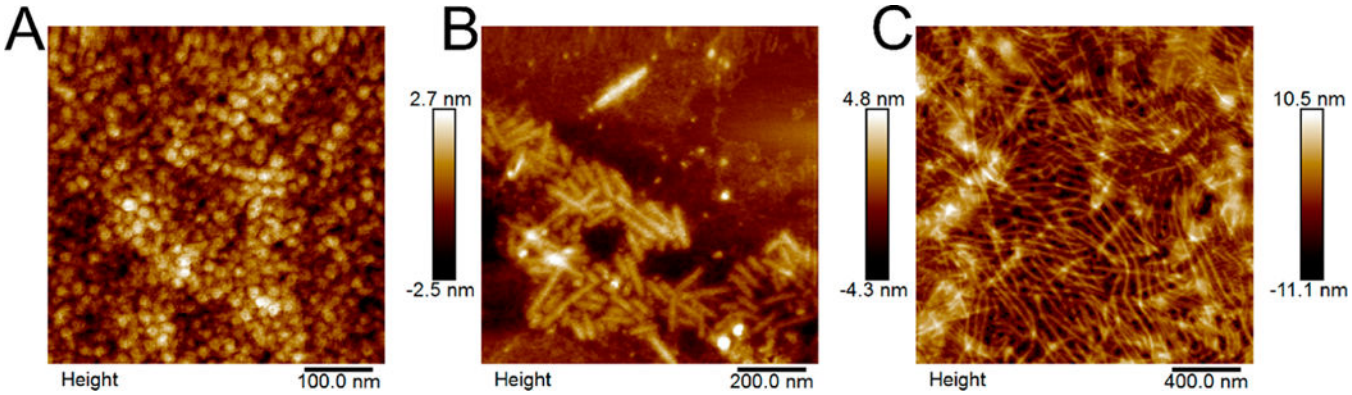

Figure 3.

rH174 nanostructures formed in SEF at acidic pH progress from nanospheres at 1 day (A) to nanorods with nanospheres at 1 week (B) with nanoribbons observed by 2 weeks (C) at 37 °C. Representative AFM micrographs of $n = 3$ independent syntheses.

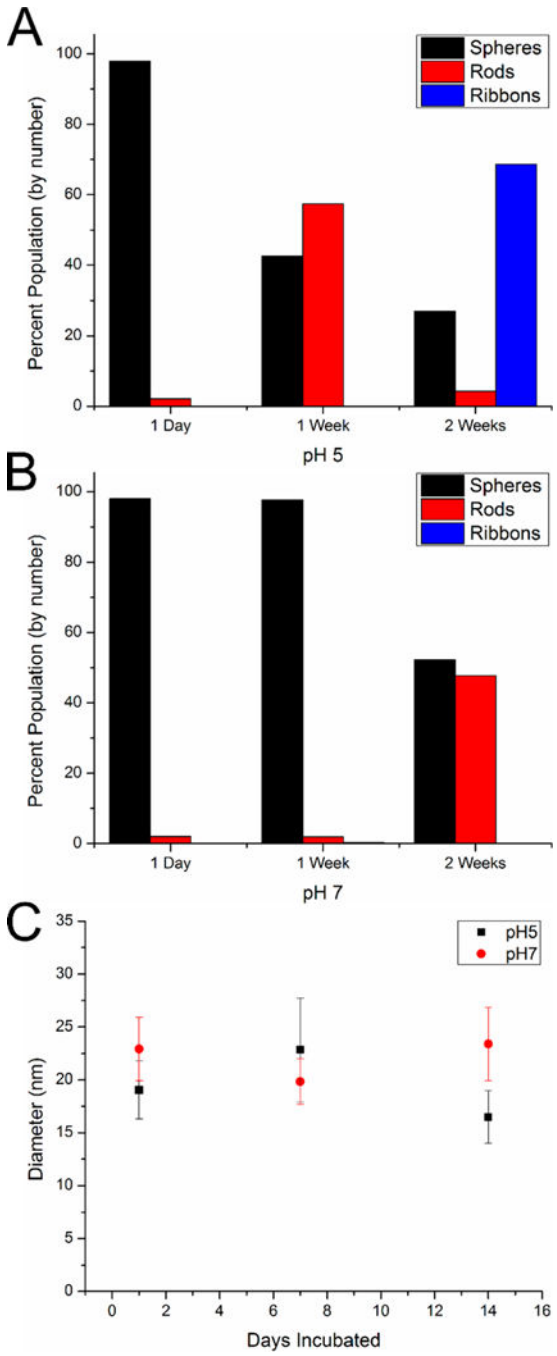

Figure 4.

Distribution of nanostructures following incubation at 37 °C in acidic (A) or alkaline (B) assembly conditions. Percent of total population by number calculated from AFM micrographs. Change in sphere diameter (C) is not significant over time (*$p > 0.05$), whereas diameter is significantly impacted (*$p < 0.001$) by assembly pH; $n = 30$ spheres; two-way ANOVA with Tukey's posthoc test.

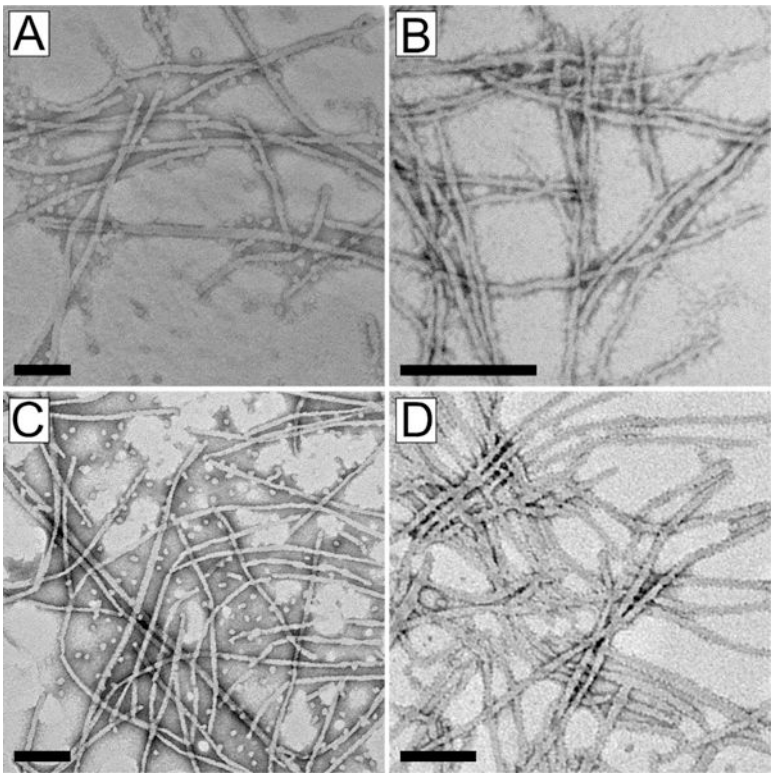

Figure 5.
TEM of rH174 nanoribbons and nanospheres remained stable together in alkaline solution after 3 weeks (A) or 8 weeks (C), whereas few nanospheres were observed in acidic conditions at 3 weeks (B) and 8 weeks (D); Scale bar, 200 nm.

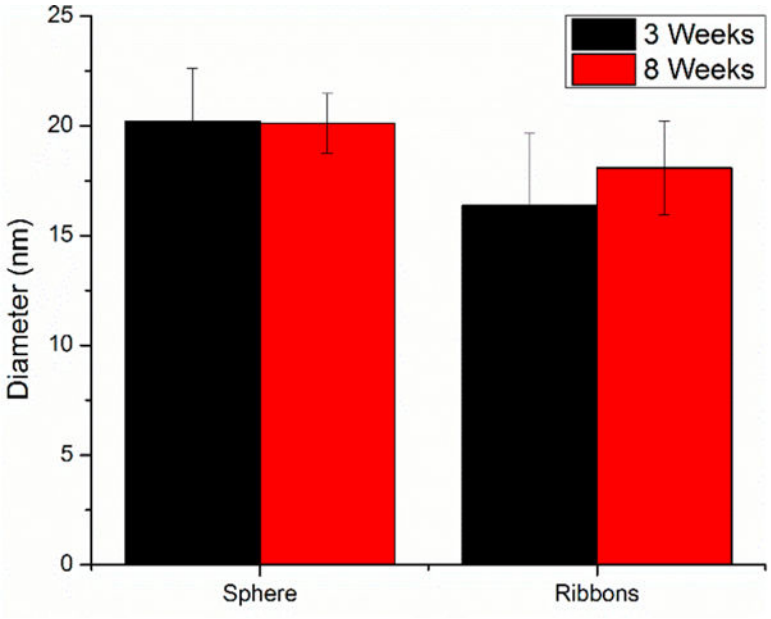

Figure 6.

Diameter of rH174 nanoribbons and nanospheres were not statistically changed between 3 and 8 weeks assembly at alkaline pH (mean and ±standard deviation measured via TEM, n = 3 structures measured for n = 3 images each; $^{*}p < 0.05$ determined by Student's t test).

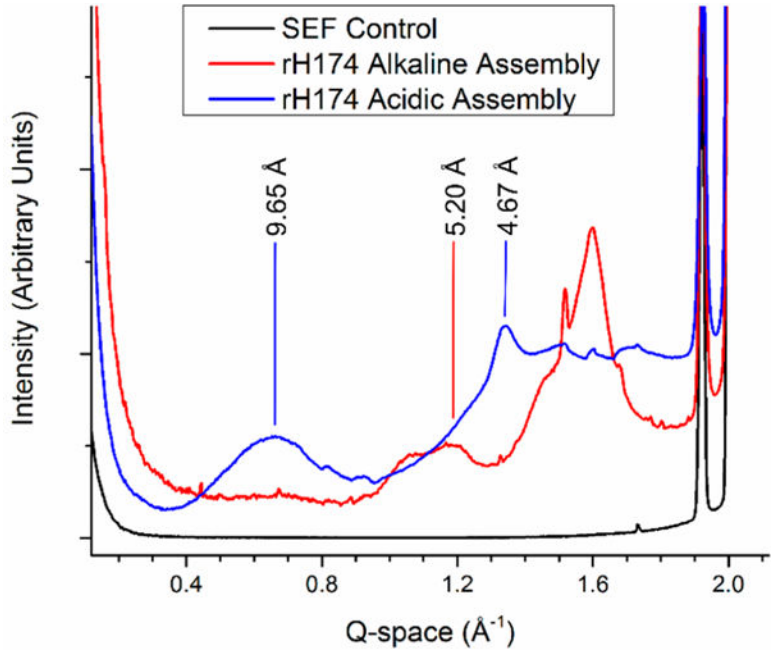

Figure 7.

XRD profile of rH174 assembled at acidic pH (blue) and alkali pH (red) have 4.67 and 5.2 Å, respectively, indicat β-sheet conformation not observed in SEF salt alone control (black). A 9.65 Å peak is indicative of antiparallel cross β-sheet amyloid stacking in rH174 assembled at acidic pH.

Table 1.

Amelogenin Self-Assembly Is Dependent on Buffer, Ionic Components, pH, and Temperature

structures obsd	dimensions[a] (nm)	buffer	ionic components (mM)	pH	temp (°C)
assessment of physiological porcine enamel[20]		enamel fluid	[Ca^{2}+] 0.15 [PO_4^{3-}] 3.9 [Na+] 139 [Mg2+] 0.8 [CO_3^{2-}] 12 [Cl^-] 150 [F^-] 0.005 [K^+] 21	7.3	37
nanospheres[9,17]	d = 12–18	Tris-HCl	[Cl^-] 20	8.0	23
nanospheres[13]	R_H=15–18	Tris-HCl	[Cl^-] 20	8.0	5–25
nanospheres[13]	R_H = 63	Tris-HCl	[Cl^-] 20	8.0	37
nanospheres[11]	R_H = 4, 12	sodium acetate	[Na^+] 20 [$C_2H_3O_2^-$] 20	5.9	23
nanospheres[11]	R_H = 5, 20	sodium phosphate	[Na^+] 60 [PO_4^{3-}] 20	8.0	23
nanospheres[21]	d = 15–20	phosphate buffered saline	[PO_4^{3-}] 4.7 [Na^+] 63 [Cl^-] 56 [K^+] 1.8	8.0	23
Nanospheres[22]	R_H= 17	phosphate buffered saline	[PO_4^{3-}] 4.7 [Na^+] 63 [Cl^-] 56 [K^+] 1.8	7.4	23, 37
nanospheres aligned linearly[18,23]	R_H = 13–27	sodium acetate	[Na^+] 25 [$C_2H_3O_2^-$] 25	4.5	20
circular/hexagonal assemblies aligned linearly[19]	d = 20	Tris-HCl	[Cl^-] 40	7.4	23
nanoribbons[24,25]	w =17	water–octanol (oil)	[Ca^{2+}] 33 [PO_4^{3-}] 20	4.5–5.5	37
nanoribbons[24]	w =17	water–octanol (oil)	[Ca^{2+}] 3.3 [PO_4^{3-}] 2.1	7.4	37
Nanoribbons[26–28]	w =17	distilled water	[Ca^{2+}] 33 [PO_4^{3-}] 20	4.5–5.5	37

[a] R_H corresponds to hydrodynamic radius as measured by dynamic light scattering (DLS), diameter (d) or width (w), as measured by AFM and/or TEM analyses